the plant journal

SEB SOCIETY FOR EXPERIMENTAL BIOLOGY

The Plant Journal (2021) doi: 10.1111/tpj.15429

Thioredoxins *m* are major players in the multifaceted light-adaptive response in *Arabidopsis thaliana*

Antonio J. Serrato[1,*], José A. Rojas-González[1], Diego Torres-Romero[2], Paola Vargas[1], Ángel Mérida[2] and Mariam Sahrawy[1]

[1]*Departamento de Bioquímica, Biología Celular y Molecular de Plantas, Estación Experimental del Zaidín (EEZ), Consejo Superior de Investigaciones Científicas (CSIC), Granada 18008, Spain, and*

[2]*Instituto de Bioquímica Vegetal y Fotosíntesis (IBVF), Universidad de Sevilla y Consejo Superior de Investigaciones Científicas (CSIC), Seville 41092, Spain*

Received 27 August 2020; accepted 15 July 2021.
*For correspondence (e-mail aserrato@eez.csic.es).

SUMMARY

Thioredoxins (TRXs) are well-known redox signalling players, which carry out post-translational modifications in target proteins. Chloroplast TRXs are divided into different types and have central roles in light energy uptake and the regulation of primary metabolism. The isoforms TRX *m1*, *m2*, and *m4* from *Arabidopsis thaliana* are considered functionally related. Knowing their key position in the hub of plant metabolism, we hypothesized that the impairment of the TRX *m* signalling would not only have harmful consequences on chloroplast metabolism but also at different levels of plant development. To uncover the physiological and developmental processes that depend on TRX *m* signalling, we carried out a comprehensive study of Arabidopsis single, double, and triple mutants defective in the TRX *m1*, *m2*, and *m4* proteins. As light and redox signalling are closely linked, we investigated the response to high light (HL) of the plants that are gradually compromised in TRX *m* signalling. We provide experimental evidence relating the lack of TRX *m* and the appearance of novel phenotypic features concerning mesophyll structure, stomata biogenesis, and stomatal conductance. We also report new data indicating that the isoforms of TRX *m* fine-tune the response to HL, including the accumulation of the protective pigment anthocyanin. These results reveal novel signalling functions for the TRX *m* and underline their importance for plant growth and fulfilment of the acclimation/response to HL conditions.

Keywords: thioredoxins, *Arabidopsis thaliana*, chloroplast, light acclimation, redox regulation, chlorophyll fluorescence, anthocyanins.

INTRODUCTION

Thioredoxins (TRXs) are redox-signalling proteins present in almost all living organisms. These small proteins (12–14 kDa) share a very conserved tertiary structure and have an active site containing two reactive cysteines (CxxC). Their biological function mostly consists of reducing target proteins, thus acting as molecular redox switchers by transferring electrons to a pair of disulphide-bonded cysteines. Two main features determine their target specificity: redox potential and electrostatic surface potential (Collin et al., 2003).

Plant TRXs are distributed throughout different organelles such as nuclei, mitochondria, and chloroplasts (Meyer et al., 2009). Chloroplast TRXs are nucleus-encoded proteins that receive electrons from the ferredoxin thioredoxin reductase, which is in turn reduced by the ferredoxin, the last electron acceptor of the photosynthetic electron transport chain (PETC; Schürmann and Buchanan, 2008). There are several types of TRXs within the chloroplast. The *m*-type TRX was originally described as an activator of the enzyme NADP-malate dehydrogenase. Furthermore, chloroplasts contain other TRXs with an eukaryotic origin, such as types *x*, *y*, and *z*, although the best known is the *f*-type TRX, which regulates the Calvin–Benson cycle enzymes (Kang et al., 2019; Lemaire et al., 2007; Naranjo et al., 2016; Serrato et al., 2013).

The model plant *Arabidopsis thaliana* contains four isoforms of TRX *m*, namely TRX *m1*, *m2*, *m3*, and *m4*. While it has been reported that the TRX *m3* has a separated function (Benitez-Alfonso et al., 2009), the other TRX *m* regulate photosynthesis-related processes in chloroplasts where they are the most abundant TRX isoforms (Nikkanen

and Rintamäki, 2019; Nikkanen et al., 2016; Okegawa and Motohashi, 2015; Wang et al., 2013). In rice and Arabidopsis, a decrease in the TRX *m* content leads to an impairment of plant growth, chloroplast development, and photosynthesis performance (Chi et al., 2008; Okegawa and Motohashi, 2015). TRX *m* can transfer reducing power to the TRX-like protein HCF164, in the thylakoid lumen, via the thylakoid membrane protein CCDA (Kang and Wang, 2016; Karamoko et al., 2011; Motohashi and Hisabori, 2006, 2010). In addition to HCF164, it has been proposed that another lumen TRX-like protein, Suppressor Of Quenching 1 (SOQ1), is another CCDA target (Brooks et al., 2013). More than 40% of the lumen proteins can form disulphide bonds, highlighting the importance of redox regulation in this subcellular compartment (Kang and Wang, 2016). For instance, the enzyme violaxanthin de-epoxidase (VDE), a player in the activation of non-photochemical quenching (NPQ) in response to a high light (HL) stress, is redox regulated (Hallin et al., 2015; Simionato et al., 2015). On the other hand, the presence of TRX *m* in non-photosynthetic organs, such as roots and flowers, points to the regulation of other plant processes in addition to photosynthesis (Barajas-López et al., 2007). It is probable that these proteins might concertedly regulate a significant number of physiological processes. Nevertheless, a specific function has been reported for TRX *m4* in the regulation of the NADPH dehydrogenase (NDH) complex (Courteille et al., 2013) and the dually localized TRX *m2* has been proposed to regulate the voltage-dependent anion channel 3 (AtVDAC3) protein in mitochondria (Zhang et al., 2015). It seems evident that evolutionary pressure has favoured the emergence and preservation of several TRX *m* isoforms in plants.

Plants are continuously sensing light intensity and quality to adjust their own growth and development. In photosynthetic tissues, the light-dependent retrograde signalling relies on redox players acting at the level of the PETC (Gollan et al., 2015). Key components of the redox-signalling pathways are the members of the chloroplast TRX family (Gütle et al., 2017; Serrato et al., 2013). TRX *m* plays a significant role in maintaining a proper PETC, participating in the assembly and protection of photosynthesis complexes (Courteille et al., 2013; Kang and Wang, 2016; Wang et al., 2013). Some authors have also addressed the role of the TRX *m1* and *m2* in photosynthesis regulation in fluctuating light (Thormählen et al., 2017). Including TRX *m4* in further studies would lead to a more comprehensive knowledge of this issue.

The chloroplast redox state is vital for plant physiology and development, but knowledge on this issue is still very limited. As the TRX *m* are major redox players in the chloroplast, we wanted to gain more insight into their role in the regulation of chloroplast processes as well as their involvement in the control of extra-chloroplast processes through retrograde signalling. As redox regulation in the chloroplast is intimately bound to light, we designed and implemented a set of light-dependent experimental approaches to obtain multilevel information based on the characterization of Arabidopsis mutant lines grown under optimal (normal redox pressure) or HL (high redox pressure) conditions. In this research context, and in addition to carrying out a physiological and phenotypic characterization in standard growth conditions, our work has also been focused on analysing (i) long-term HL acclimation, and (ii) short-term responses to HL treatments in TRX *m*-deficient lines. We report novel and comprehensive information and discuss the importance and isoform specificities of the redox regulation mediated by TRX *m* for leaf architecture, gas exchange, activation of energy dissipation mechanisms, and anthocyanin accumulation in response to HL.

RESULTS

Mutations of Arabidopsis TRX *m1, m2,* and *m4* impair the rosette growth, particularly under HL conditions

Taking advantage of the specific antibodies that we obtained, we determined the TRX *m* level in the different *trxm* genetic backgrounds (Figure S1). Compared with wild-type (WT) plants, the single *trxm* mutants showed either a non-detectable signal (*trxm1* and *trxm4*) or very reduced levels (*trxm2*) of the affected TRX *m* isoform, as we similarly reported at a transcript level in a previous article (Fernández-Trijueque et al., 2019). As previously stated by other authors (Wang et al., 2013), the content of TRX *m2* in the double and triple mutants turned out to be higher than in the single mutant (Figure S1), probably to compensate the redox deficiencies provoked by the lack of the other isoforms. On the other hand, TRX *m4* was not detected in the lines containing the *trxm4* allele and the isoform TRX *m1* showed very faint signals in the lines *trxm1m4* and *trxm1m2m4*. With these results, we confirmed that all the *trxm* lines that we isolated and analysed in this study were defective in the redox signalling mediated by TRX *m*.

We next compared the growth rate of the *trxm* mutants under two light conditions: an optimal growth light (GL) intensity (120 μmol photons m^{-2} sec^{-1}) and a challenging HL treatment (700 μmol photons m^{-2} sec^{-1}). Rosettes were sampled and quantified every 5 days throughout the vegetative growth of the Arabidopsis plants (Figure 1). At first glance, some lines displayed a developmental delay in both light conditions, particularly the Arabidopsis lines *trxm1m4*, *trxm2m4*, and *trxm1m2m4* (Figure 1a). Confirming our *de visu* observations (Figure 1b), adult plants of the mutants *trxm1m4*, *trxm2m4*, and *trxm1m2m4* produced less biomass than the WT line in the GL condition (38%, 15%, and 42%, respectively). Interestingly, the

mutant line *trxm1* and, to a lesser extent, the line *trxm1m2*, weighted more than the WT line at the end of the vegetative growth when cultivated in GL.

Regarding the HL treatment, excepting the lines *trxm1* and *trxm1m2*, the mutant lines produced less biomass than the WT plants (Figure 1b). This was particularly marked in the triple mutant. Despite mutant growth being compromised by HL, we did not observe any upregulation of the TRX *m* in response to HL (Figure S2).

Unexpectedly, the differences observed with the area were not as evident as with the weight quantifications, as the rosette areas of the mutant lines *trxm1m4* and *trxm1m2m4* were more similar to the control line (Figure 1c). To uncover putative alterations in the leaf mass per area (LMA), we represented the rosette area versus the fresh weight (Figure 1d). The plotted scattered points fitted well to straight lines ($R^2 \geq 0.99$), as previously reported by other authors (Massonnet et al., 2010). The LMA values were lower in the double mutants, *trxm1m4* and *trxm2m4*, and in the triple mutant than in the WT line in GL. The differences in LMA increased even more with the HL treatment, observing higher differences between the WT line

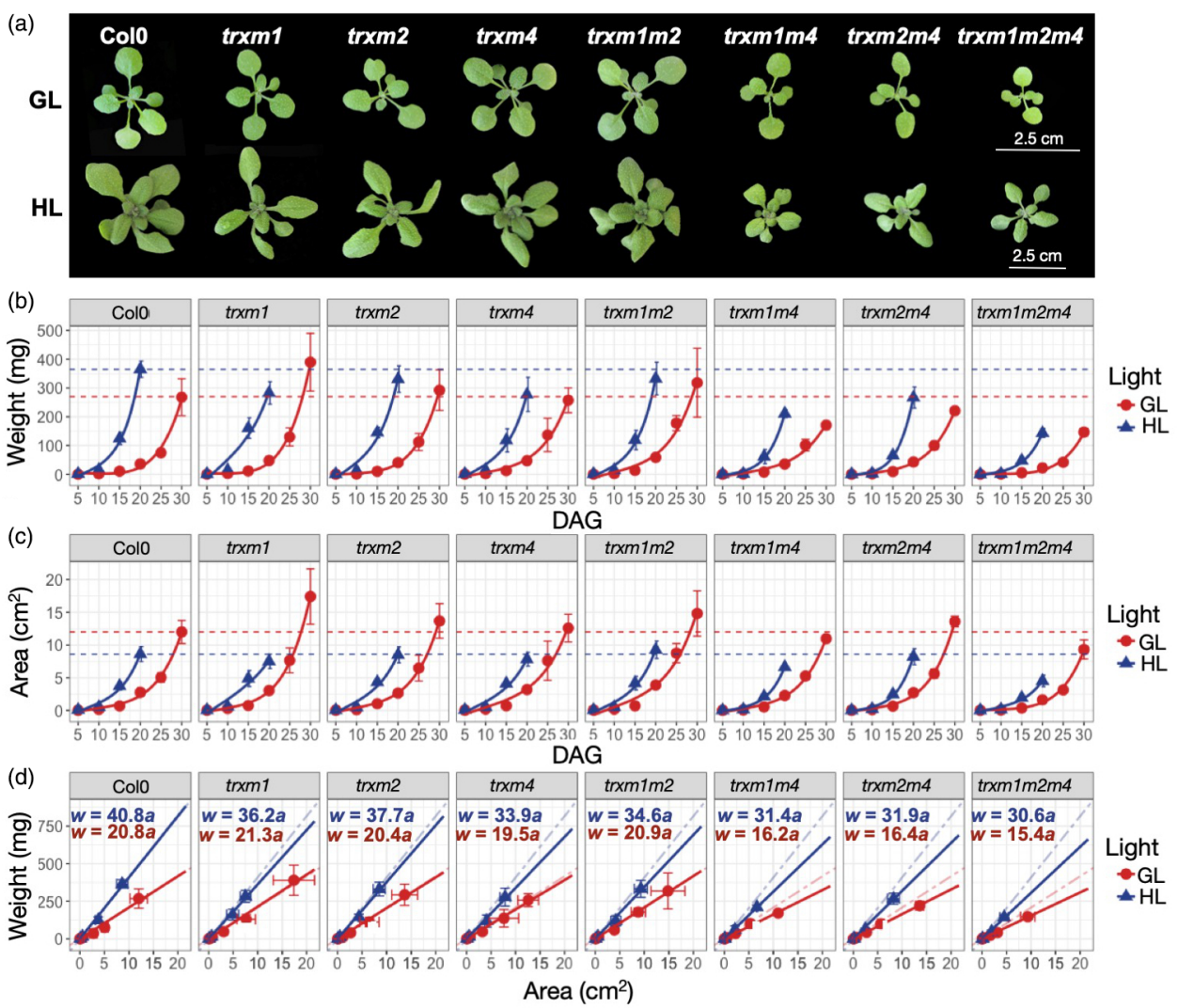

Figure 1. Phenotypic characterization of wild-type (Col0) and *trxm* lines.
(a) Fifteen-day-old plants cultivated in normal growth light (GL) conditions or in high light (HL) conditions.
(b) Growth curves representing the rosette fresh weight.
(c) Growth curves representing the projected rosette area.
(d) Relationship between the area and the fresh weight of WT and *trxm* lines. Regression lines for the weight (*w*) and the area (*a*) are shown in the upper left corner of the graphs. Calculated regression coefficients represent the leaf mass per area. Coefficients of determination (R^2) were ≥0.99. Plants were sampled every 5 days from the 5th to the 30th day after germination (DAG) for GL or until the 20th DAG for HL. Values are mean ± standard error of five independent plant samples.

The Plant Journal, (2021), doi: 10.1111/tpj.15429

and the double mutants than with the single ones (Figure 1d). To sum up, (i) mutant alleles triggered physical changes in the leaf structure, and (ii) Arabidopsis development was particularly impaired in the *trxm* mutants in HL, being more evident when the isoform TRX *m4* was lacking.

Remodelling of the mesophyll structure in *trxm* mutants

Arabidopsis lines grown in GL showed thinner leaves than those cultivated in HL (Figure 2) (Hoshino et al., 2019). Cross-sectional areas of the leaves with a light microscope showed evident differences (Figure 2). The mutant line *trxm2* apparently had small palisade-mesophyll cells, while the *trxm1m4* mutant displayed a larger size compared with the WT line grown in GL conditions. To carry out a statistical analysis, we quantified and compared the area of the cross-sectioned cells as an indicative parameter for cell size (Figure 2). Quantifications revealed that the GL-grown mesophyll cells of the single mutants *trxm2* and *trxm4* and the double mutant *trxm1m2* were smaller than those of the WT line were. On the contrary, the mesophyll of the double mutant *trxm1m4* displayed a bigger cell cross-sectional surface compared with the WT line. Remarkably, in contrast to the GL condition, the mesophyll-cell area of the single mutant *trxm4* increased with respect to the WT line in the HL condition. Lines *trxm1* and *trxm2m4* also showed bigger mesophyll cells than the control line in HL. The most contrasting observation occurred with the *trxm1m4* mutant, which showed the greatest cell size in GL, but the lowest one in HL. To uncover a putative interconnection between light and TRX *m* signalling and its effect on the leaf structure, we calculated the difference in size of mesophyll cells in both light conditions (ΔArea; Figure 2). Under our experimental conditions, both WT palisade and spongy cells were smaller in HL than in GL conditions. This light response indicated that, together with an increase in the mesophyll thickness (Figure 2), a moderate reduction in the cell size was occurring in response to a high irradiance as part of the plant acclimation process. Nonetheless, *trxm* single mutants behaved in the opposite way and increased their cell size when plants were cultivated in HL. These alterations suggested the existence of light-dependent components that might be interacting with the redox signalling mediated by TRX *m1*, *m2*, and *m4*. In contrast, the double mutant *trxm1m4* displayed an evident cell-size reduction, while the mutants *trxm1m2* and *trxm2m4* did not follow this same pattern as they showed a quite similar cell size in both light conditions (Figure 2).

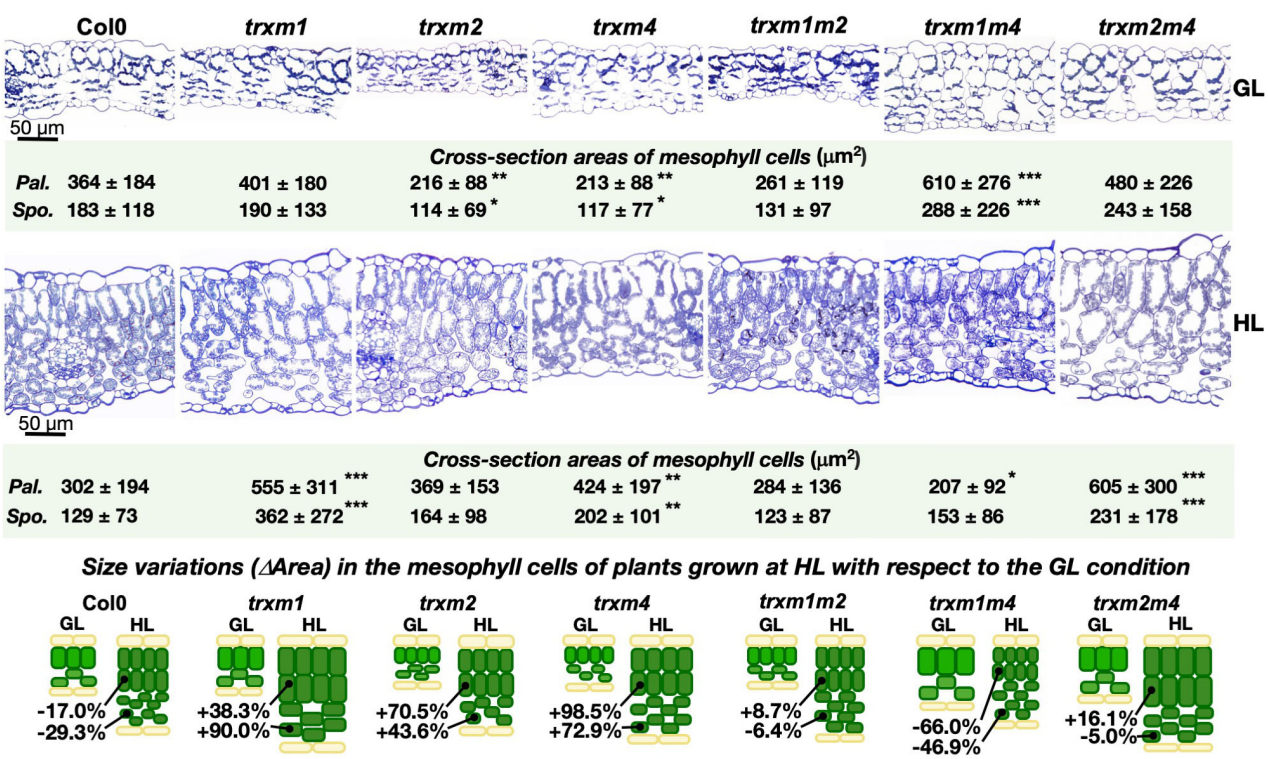

Figure 2. Light microscopy images of cross-sections of wild type (Col-0) and *trxm* mutant leaves.
Samples were taken from comparable zones of fully expanded leaves. Arabidopsis plants were grown for 21 days either at optimal growth light (GL) or in high light (HL) conditions. Semithin cross-sections of leaves were stained with toluidine blue (which stains proteins). Cell areas (samples size ranging from 37 to 197 for line and light condition) were quantified with ImageJ 2.0.0. Values are presented as means ± standard deviation. Differences with wild type were analysed using Tukey's test. Asterisks indicate that the compared mean values were statistically significant (*$P < 0.05$, **$P < 0.01$, ***$P < 0.001$).

Low levels of TRX *m* imbalance the photosynthetic gas exchange in Arabidopsis

The CO_2 assimilation rate of Arabidopsis plants grown in HL conditions was higher than in those cultivated in GL (Figure 3a), with fold increases ranging from 2.8 to 4.4 (lines *trxm1m2* and *trm1m4*, respectively) (Table S2). Moreover, we did not observe any statistically significant differences between the photosynthetic parameters of the mutant lines versus the WT line related to the CO_2 assimilation rate (Table S2). Although statistically not significant, the maximum net photosynthetic rate (A_{max}) at GL was slightly higher in the *trxm2* mutant (approximately 17% higher) and, on the contrary, it was lower in the *trxm1m4* mutant (approximately 28% lower). We want to notice that the difference of A_{max} between those mutants was statistically significant ($P < 0.02$).

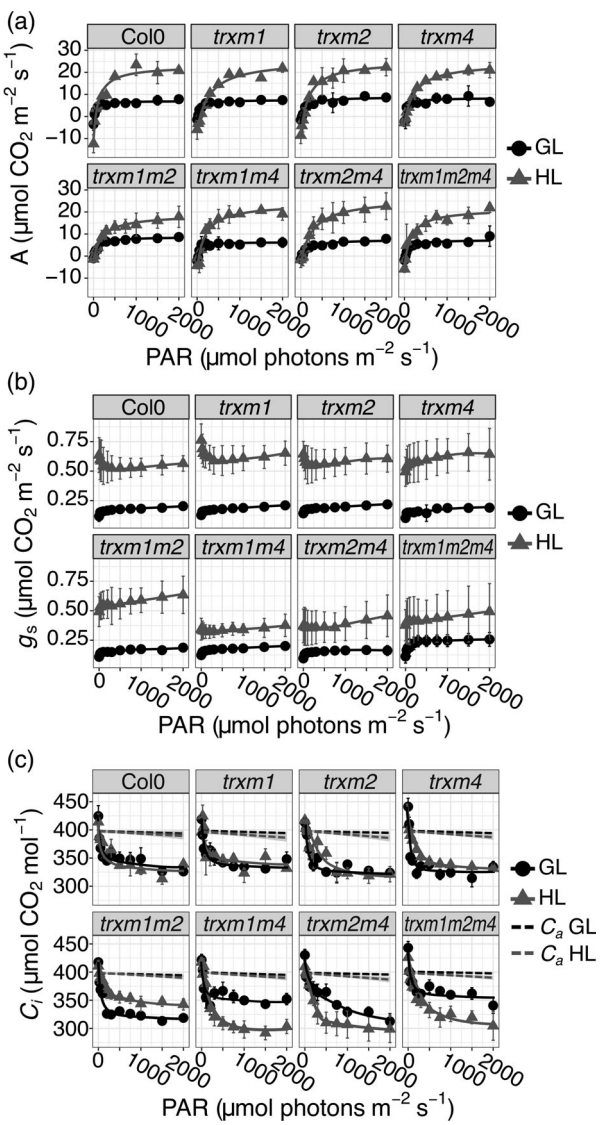

Figure 3. Infrared gas analyser measurements in wild-type (Col0) and *trxm* mutants.
(a) Light–response curves for the rate of photosynthetic CO_2 assimilation (A); (b) stomatal conductance (g_s); and (c) intercellular CO_2 concentration (C_i). Arabidopsis plants were grown for 4 weeks at optimal growth light (GL) or for 3 weeks in high light (HL) conditions. Ambient CO_2 concentration (C_a) was adjusted to 396.4 ± 0.3 µmol CO_2 mol^{-1} (dashed lines). Values are mean ± standard error of three independent plants.

In GL conditions, the triple mutant displayed the highest stomatal conductance (g_s) (Figure 3b). The lines WT, *trxm1*, and *trxm2* showed a distinctive curve profile consisting of a dramatic transpiration decay spanning from 0 to 250 µmol photons m^{-2} sec^{-1} of light intensity, followed by a steady linear increase. This g_s profile was different in the other lines analysed, as the initial drop was not observed. The leaf intercellular CO_2 concentration was above 300 ppm in all lines (Figure 3c) and suggested that g_s was not responsible for the lower A_{max} showed by some mutants.

Apart from mutants, *trxm1m4*, *trxm2m4*, and *trxm1m2m4*, grown at HL (dashed circle), intrinsic water-use efficiency (iWUE) and LMA seemed to be positively correlated (Figure 4a). As the stomata are key structures controlling leaf gas exchange, we wondered whether there were alterations in the stomata of the mutant lines exhibiting the lowest iWUE (bold names in Figure 4a). For this purpose, we compared the stomatal pattern of the *trxm1m4* and triple mutants with that of the WT line grown in GL (Figure 4). Both the epidermal cells and the stomata showed a normal morphology (Figure 4b); nevertheless, contrary to the WT leaves, which displayed a lower stomata number on the adaxial side (approximately 225 stomata/mm^2) than on the abaxial side (approximately 320 stomata/mm^2), the two mutants analysed had a similar stomata number on both sides (190–200 stomata/mm^2, Figure 4c). The low stomata number in the mutants *trxm1m4* and *trxm1m2m4* contrasted with the WT-like stomatal conductance measured with infrared gas analyser (Figure 4c). With respect to the stomata length, while the stomata of the adaxial side were slightly smaller (approximately 10%), the abaxial side presented slightly bigger stomata (approximately 10%) than the control line (Figure 4d). As far as the aperture was concerned, the mutant lines showed slightly more closed stomata than those of the WT line (Figure 4e). These results did not explain the low iWUE observed in these mutants cultivated at GL; however, they pointed to an unreported role of the redox signalling mediated by TRX *m* in the stomata differentiation.

Apart from analysing the photosynthetic CO_2 assimilation capacity (photochemical quenching), we also investigated how efficiently photosynthesis was carried out in the *trxm* mutants. For this purpose, we determined the maximum quantum yields of photosystem (PS)II (F_v/F_m) by chlorophyll fluorescence measurements. F_v/F_m was statistically significant lower in the double mutant *trxm1m4* and the triple mutant with respect to the WT line in both light

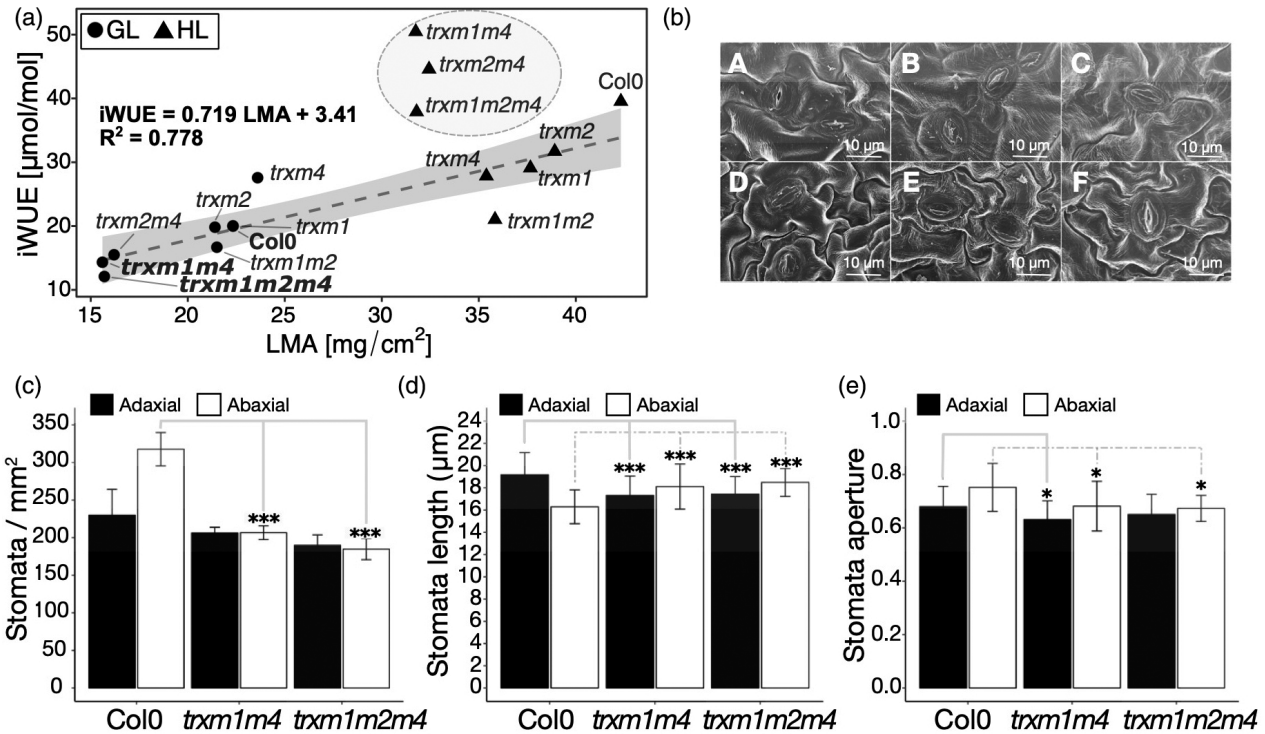

Figure 4. Stomatal characterization in wild-type (Col0), *trxm1m4*, and *trxm1m2m4* plants grown in normal light conditions.
(a) Correlation between leaf mass per area (LMA) and intrinsic water-use efficiency (iWUE).
(b) Representative scanning electron microscope images of adaxial (a–c) and abaxial (d–f) epidermis of wild-type (a,b), *trxm1m4* (b,e), and *trxm1m2m4* (c,f) plants.
(c) Stomatal density of the adaxial and abaxial leaf epidermis.
(d) Stomata length of the adaxial and abaxial leaf epidermis.
(e) Stomatal aperture calculated as the width/length ratio. Values shown for iWUE correspond to 120 µmol photons m^{-2} sec^{-1} PAR (GL) and to 700 µmol photons m^{-2} sec^{-1} PAR (HL). Regression line for LMA and iWUE, together with the coefficient of determination (R^2), are shown in the graph. Stomata width and length were measured with ImageJ 2.0.0. Represented values are mean ± standard deviation. $^*P < 0.05$, $^{***}P < 0.01$ as analysed by one-way analysis of variance followed by a Tukey's *post hoc* test. $n = 50$ per genotype.

conditions (Table 1). These results suggest the occurrence of underlying light–energy imbalances and prompted us to gain more insight into how efficiently *trxm*-mutant plants were managing light energy uptake and dissipation under a HL situation.

Energy dissipation mechanisms or changes in the redox poise of PSII in response to HL are differentially regulated by the TRX *m* isoforms

To know how TRXs *m* were regulating the plant response to HL, Arabidopsis double and triple mutants were grown in GL for 3 weeks and then subjected to a 2-day HL treatment (500 µmol photons m^{-2} sec^{-1}). By using an Imaging-PAM fluorometer, we analysed the chlorophyll fluorescence to find out the PSII performance (Figures 5 and 6). As we had previously observed (Table 1), in dark-adapted plants the maximum quantum yields of PSII (F_v/F_m) were lower in the lines *trxm1m4* and *trxm1m2m4* than in the WT plants under non-stress conditions (Figure 5). However, after the HL treatment, the F_v/F_m ratios were significantly lower in the mutants *trxm1m4*, *trxm2m4*, and *trxm1m2m4* than in the WT or *trxm1m2* lines (Figure 5). According to these data, the maximum efficiency of PSII was primarily dependent on the regulation exerted by the TRX *m4* isoform and, to a lesser extent, by the TRX *m1* or *m2* isoforms.

We next analysed the chlorophyll fluorescence of light-adapted plants subjected to a HL treatment (Figure 6). To allow a more precise analysis, we calculated the distances between the light–response curves ("dm" values in Figure 6). Regarding the PSII quantum yield [Y(II)] and the NPQ, apart from the triple mutant, the double mutants *trxm1m4* and *trxm2m4* showed the highest differences with respect to the WT line (Figure 6a,b). The fraction of closed reaction centres in PSII ($1 - q_L$) in the mutant *trxm1m2* showed values similar to that of WT, while the rest of the lines were not as efficient in the Q_A reduction, particularly the triple mutant (Figure 6c).

Conversely to the GL condition, the Arabidopsis mutants showed a significant decrease in Y(II) in parallel with an increase in NPQ after 2 days of HL treatment. The Y(II) and NPQ curve profiles were noticeably different to those of

Table 1 Photosystem II efficiency of the wild-type (Col0) and *trxm* mutant lines grown at GL and HL

Line	F_v/F_m GL	F_v/F_m HL
Col-0	0.830 ± 0.002	0.822 ± 0.007
trxm1	0.830 ± 0.005	0.827 ± 0.005
trxm2	0.833 ± 0.002	0.826 ± 0.003
trxm4	0.826 ± 0.003	0.822 ± 0.009
trxm1m2	0.829 ± 0.002	0.826 ± 0.009
trxm1m4	0.811 ± 0.008*	0.752 ± 0.029*
trxm2m4	0.827 ± 0.003	0.811 ± 0.012
trxm1m2m4	0.804 ± 0.009*	0.732 ± 0.009*

Measurements were performed as described in the "Experimental procedures" section. Values are means ± standard deviation of five independent plant samples. Differences with wild type were analysed using Tukey's test. Twenty-one-day-old plants cultivated in normal GL or in HL conditions.
GL, growth light; HL, high light.
*Compared mean values were statistically significant ($P < 0.001$).

the WT and *trxm2m4* lines (Figure 6a,b). These differences were even higher after a 24-h recovery period in GL, when the HL stimulus was no longer present. According to our results, TRX *m1* was more important than TRX *m2* or *m4* in maintaining the Y(II) performance, as the redox activity in the mutant line *trxm2m4* displayed a WT-like NPQ in response to HL (Figure 6b). Remarkably, these differences were restricted to light intensities below 600 μmol photons m^{-2} sec^{-1}. On the other hand, the mutants *trxm1m4*, *trxm2m4*, and *trxm1m2m4* suffered a drop in $1 - q_L$, particularly dramatic in the triple mutant, suggesting a problem in the reduction of Q_A that might affect the redox state of the plastoquinone pool. Contrary to the Y(II) and NPQ parameters, it seems that the TRX *m4* isoform is more important than the other isoforms to reach a proper Q_A reduction in the plant response to HL. Conversely, after a recovery time of 24 h in GL, the mutant lines bearing the *trxm2* mutant allele (*trxm1m2*, *trxm2m4*, and *trxm1m2m4*) exhibited higher differences with respect to the WT line than the mutant *trxm1m4*, bearing the WT allele *TRXm2* (Figure 6c). The recovery pattern of the mutant lines indicated that TRX *m2* is somehow involved in the Arabidopsis acclimation back to lower light conditions.

Finally, 1 week after the HL treatment, all the parameters analysed recovered the initial control values (Figure 6). In conclusion, our experimental data indicated that Y(II) and NPQ, on the one hand, were mainly regulated by the TRX *m1* isoform, while the maximum quantum yield of PSII and the reduction of Q_A were mostly regulated by the TRX *m4* isoform. The role of the TRX *m2* was not as evident as for the other two isoforms. However, we cannot rule out its involvement in the response to HL. The absence of a clear phenotype in the single *trxm* mutants (Figure S3) strongly suggests that, with respect to the issues that we were studying, one of the TRX *m* isoforms may play a leading role in the regulation of the photosynthesis-related processes while the other two isoforms could provide a less efficient redox assistance.

After observing the unusually increased NPQ in the HL-treated mutants, we realized that this energy release might be related to a parallel increase in leaf temperature. Therefore, we decided to examine the leaf temperatures of the Arabidopsis lines grown in GL and HL of the photosynthesis analyses previously described in Figure 3. In GL grown plants, leaf temperatures (measured with the infrared gas analyser temperature sensor) adjusted well to a linear model ($R^2 > 0.95$) with a positive slope (Figure 7). On the contrary, in the HL grown plants, not all the lines adjusted well to a linear model and only the WT line and the single mutants *trxm1* and *trxm2* displayed a high regression coefficient ($R^2 > 0.95$). Among the single mutants, only *trxm4* showed a distinctive temperature profile. The double-mutant curves did not adjust well to a linear model, particularly the *trxm1m4*, *trxm2m4*, and *trxm1m2m4* lines, with R^2 values of 0.736, 0.845, and 0.725, respectively. Another feature related to the single mutant *trxm4* and double *trxm* mutants was the lower leaf thermal amplitude along the light curve (37% lower in the triple mutant with respect to the control line). These lines displayed a typical temperature sub-peak at about 250 μmol photons m^{-2} sec^{-1}, which coincided with the one observed in the NPQ curves (Figure 6b).

Anthocyanin accumulation in response to a HL treatment is impaired in the *trxm1m4* and *trxm1m2m4* mutant lines

It is known that the chloroplast redox status plays a central role in the regulation of nuclear genes in response to environmental cues (Pfannschmidt et al., 2009). Anthocyanin is accumulated in leaves in response to HL as part of the plant protection mechanisms. To know whether TRX *m* redox signalling is involved in this physiological process, we analysed the anthocyanin content in the GL-grown *trxm* mutants after a 4-day HL treatment (Figure 8). The *trxm1m4* and *trxm1m2m4* mutants only accumulated half the content of the rest of lines (Figure 8a). When the *trxf1f2* mutant line was also submitted to the same experimental conditions, we observed a normal anthocyanin accumulation (Figure 8b), suggesting that the pigment accumulation was exclusively dependent on the signalling mediated by the TRX *m1* and *m4*.

Jasmonic acid (JA) is a key player triggering anthocyanin accumulation in response to an abiotic stress such as HL (Balfagón et al., 2019; Shan et al., 2009). As the first step of the JA biosynthetic pathway takes place in the chloroplast, we explored the possibility of JA impairment in the affected mutant lines. To rule out any blockage or downregulation of the JA accumulation in the *trxm1m4* or the triple mutants, we supplied exogenous JA with the aim of recovering a WT-like anthocyanin accumulation in the mutant plants submitted to HL treatment (Figure 8c).

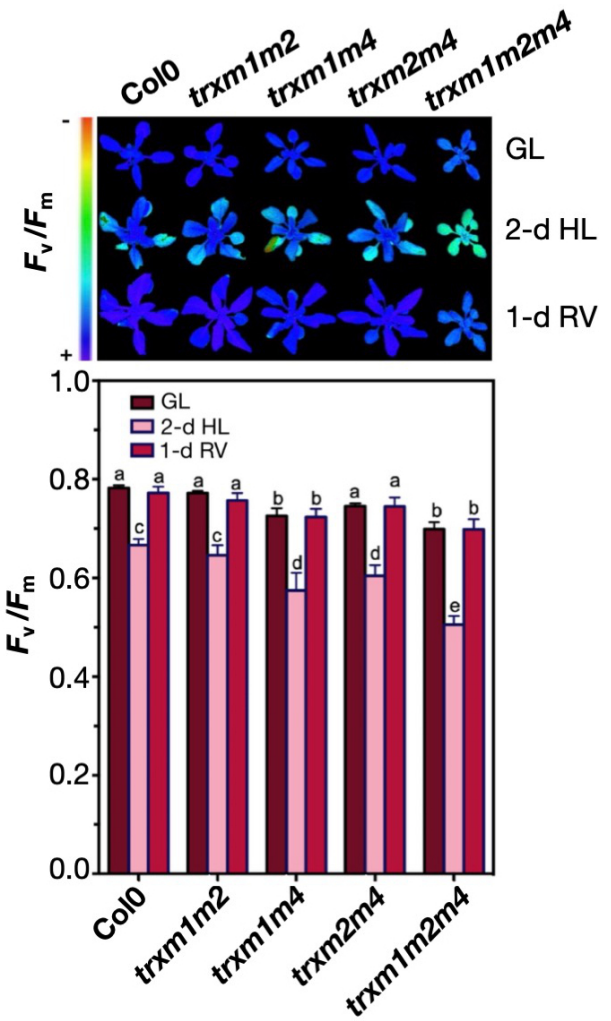

Figure 5. Photosystem II performance (F_v/F_m) in wild-type (Col0) and *trxm* double and triple mutants.
Arabidopsis lines cultivated in normal light conditions [growth light (GL)] were subjected to a 2-day high light (HL) treatment and left to recover 1 day (1-day RV) at GL. Represented values are mean ± standard error. Different letters mean statistically significant differences according to a one-way analysis of variance followed by a Tukey's *post hoc* test. Four biological replicates were performed. RV, recovery.

Although the mutant lines did not reach a WT anthocyanin content, the three Arabidopsis lines did respond to the treatment as they accumulated twice the pigment content of the non-treated plants. Furthermore, we confirmed that JA signalling was not affected either as we quantified similar anthocyanin contents when the JA treatments were carried out in GL (Figure 8d). An HL-dependent factor other than JA, and related to TRX *m*, was involved in the anthocyanin accumulation in light-stressed plants. Conversely, compared with what we had observed so far with other phenotypic traits, the mutant allele *trxm2* did not have any noticeable influence on the anthocyanin accumulation, which turned out to be TRX *m1* and *m4* dependent.

To know whether anthocyanin gene regulation was altered, we further examined transcript accumulation in the triple *trxm* mutant in response to HL (Figure 9). To this end, we analysed the mRNA levels of the biosynthesis genes *ANS*, *CHS*, and *DFR* (Figure 9a), the positive regulators *PAP1* and *TT8* (Figure 9b) and the negative regulators *ANAC032*, *MYBL2*, and *TCP15* (Figure 9c). Besides *MYBL2*, all the transcripts under study were more abundant in the triple *trxm* mutant than in the WT line. Differences were statistically significant with *ANS*, *DFR*, *ANAC032*, and *TCP15*. Interestingly, despite accumulating less anthocyanin, the biosynthesis genes that we studied were induced more in the triple *trxm* mutant.

DISCUSSION

Leaf architecture depends on TRX *m* signalling

Low TRX *m* levels in Arabidopsis mutants cause plant growth defects (Da et al., 2018; Okegawa and Motohashi, 2015). The growth assays we carried out corroborated these previous results (Figure 1). Nevertheless, beyond a lower plant growth rate, we also observed that the LMA was different in some *trxm* lines, particularly in the HL-cultivated plants (Figure 1). It seems that TRX *m4* was the most important isoform controlling the LMA as the combination of the allele *trxm4* and any of the other mutant alleles led to a decrease in LMA, which was not observed in the *trxm1m2* mutant. It is worth mentioning that TRX *m4* has been the only chloroplast TRX proposed to regulate the cyclic electron flow (CEF) (Courteille et al., 2013). CEF activation might affect the NADPH/ATP ratio and, consequently, the chloroplast metabolism and plant growth. Nevertheless, although CO_2 assimilation does not seem to be impaired (Figure 3a), other key metabolic pathways related to the leaf structure/development might be affected. LMA can be influenced by factors such as leaf thickness, mesophyll layer thickness, mesophyll cell-wall thickness, and intercellular airspace (Ren et al., 2019). However, the complex mesophyll cell-size pattern in the *trxm* mutants (Figure 2) suggests the existence of a complex and dynamic signalling network where TRX *m* might be important redox nodes.

Imbalance in the assimilated CO_2 per H_2O transpired in the *trxm* mutants

Photosynthesis did not seem to be significantly affected in the *trxm* mutants compared with the WT line (Figure 3a; Table S2). Interestingly, the triple mutant *trxm1m2m4* showed an A_{max} that was in between the values of the *trxm1m4* and *trxm2* lines. Regarding these results, it would be tempting to think that TRX *m1* and *m4* are boosting photosynthesis in GL conditions, while TRX *m2* is acting in an opposite manner. In contrast, these differences were not observed in HL. Unlike photosynthesis, stomatal

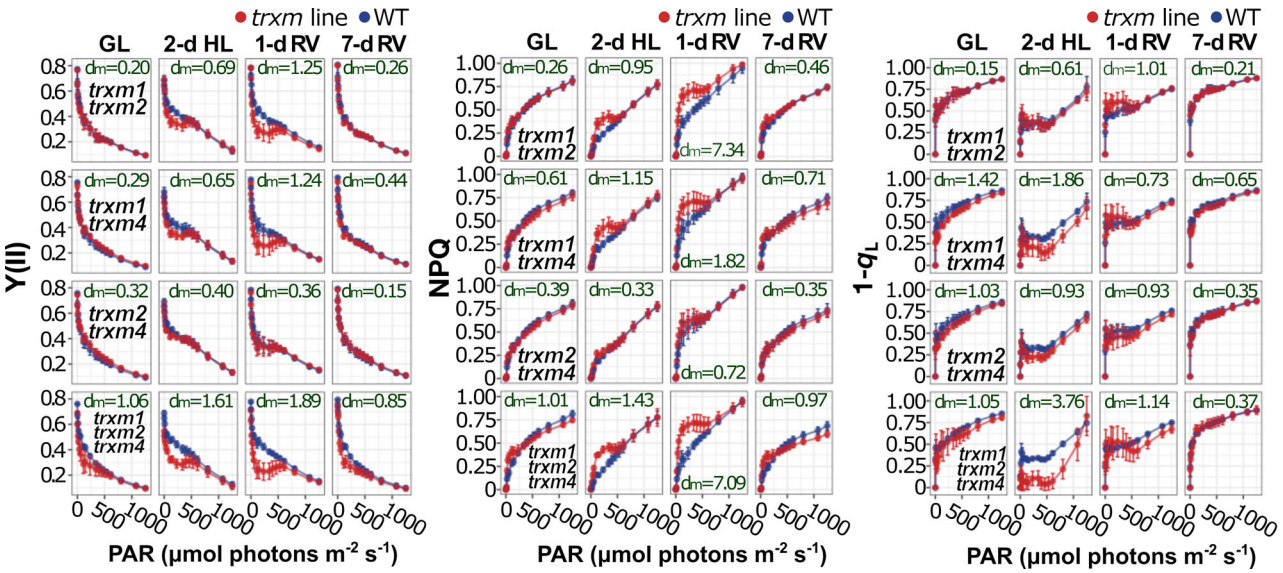

Figure 6. Light–response curves of photosystem II quantum yield [Y(II)], non-photochemical quenching (NPQ), and open reaction centres in photosystem II ($1 - q_L$) in wild-type (WT, Col-0) and double and triple *trxm* mutants.
Plants were grown in optimal growth light (GL) and then subjected to a 2-day high light (2-d HL) treatment. Plants were then taken back to GL conditions to allow stress recovery and the chlorophyll fluorescence was measured 1 day (1-d RV) and 1 week after (7-d RV). Rectilinear distance between the curves are shown as "dm" (see "Experimental Procedures" section). Data are presented as mean ± standard error. Four biological replicates were performed. PAR, photosynthetic active radiation; RV, recovery.

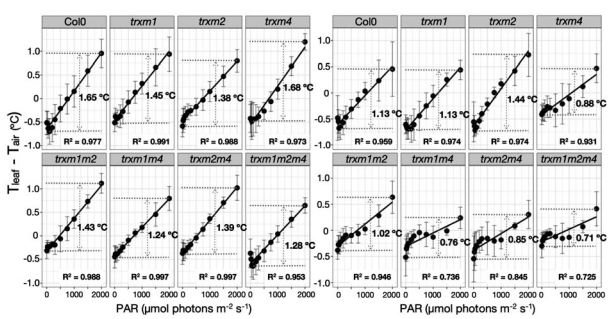

Figure 7. Light–response curve of the leaf temperature in wild-type (Col0) and *trxm* mutants.
Arabidopsis plants were grown for 4 weeks at optimal growth light (GL) or for 3 weeks in high light (HL) conditions. Temperatures were measured with an infrared gas analyser. Coefficients of determination (R^2) for the regression lines are shown. Values are mean ± standard error of three independent plants. PAR, photosynthetic active radiation; T_{air}, air temperature in the measurement chamber; T_{leaf}, temperature of the leaf.

conductance (g_s) turned out to be affected (Figure 3b). In consequence, these mutants present evident differences in iWUE, which is in correlation to LMA (Figure 4a). We have ruled out the possibility that the lower iWUE at GL was due to a higher stomata number, size, or aperture (Figure 4). On the contrary, the mutant lines were apparently counterbalancing an excessive water loss through their stomata by reducing the stomata number because of a redox imbalance. Another possibility is that a retrograde signalling via TRX *m* regulates leaf traits such as the mesophyll structure or the stomata biogenesis. The question arises as to whether the elucidation of the regulation mechanisms might become a useful biotechnological tool for improving drought tolerance in plants.

Energy dissipation is enhanced in TRX *m*-deficient plants

The increase in light intensity provoked a lineal increase in the leaf temperature in the WT line (Figure 7). The temperature curves were very similar to the NPQ curves obtained with the double and triple mutants subjected to an HL treatment (Figure 6). As occurred for the temperature peak, an NPQ peak with a photosynthetic active radiation (PAR) of 250 µmol photons m^{-2} sec^{-1} was also detected. As we could observe similar curve profiles by using different experimental approaches, this reinforces the idea that TRX *m* regulation is behind this energy-dissipation issue. Thus, it seems logical to think that the energy dissipation via NPQ and the temperature increases are linked. The question is whether these mutant plants need to dissipate more excess energy than WT plants when they are illuminated with light intensities below 600 µmol photons m^{-2} sec^{-1} and, conversely, behave as WT plants at higher light intensities. In plants, the energy-dependent quenching (qE) is the major and most rapid component of the NPQ (Müller et al., 2001). The regulation of qE involves several factors, such as a pH gradient across the thylakoid membrane (ΔpH) and the xanthophyll cycle. The thylakoid membrane complexes NDH (NDH complex) and PGR5 (proton gradient regulation complex) are involved in the ΔpH formation in the CEF (Laughlin et al., 2019; Munekage et al., 2002, 2004;

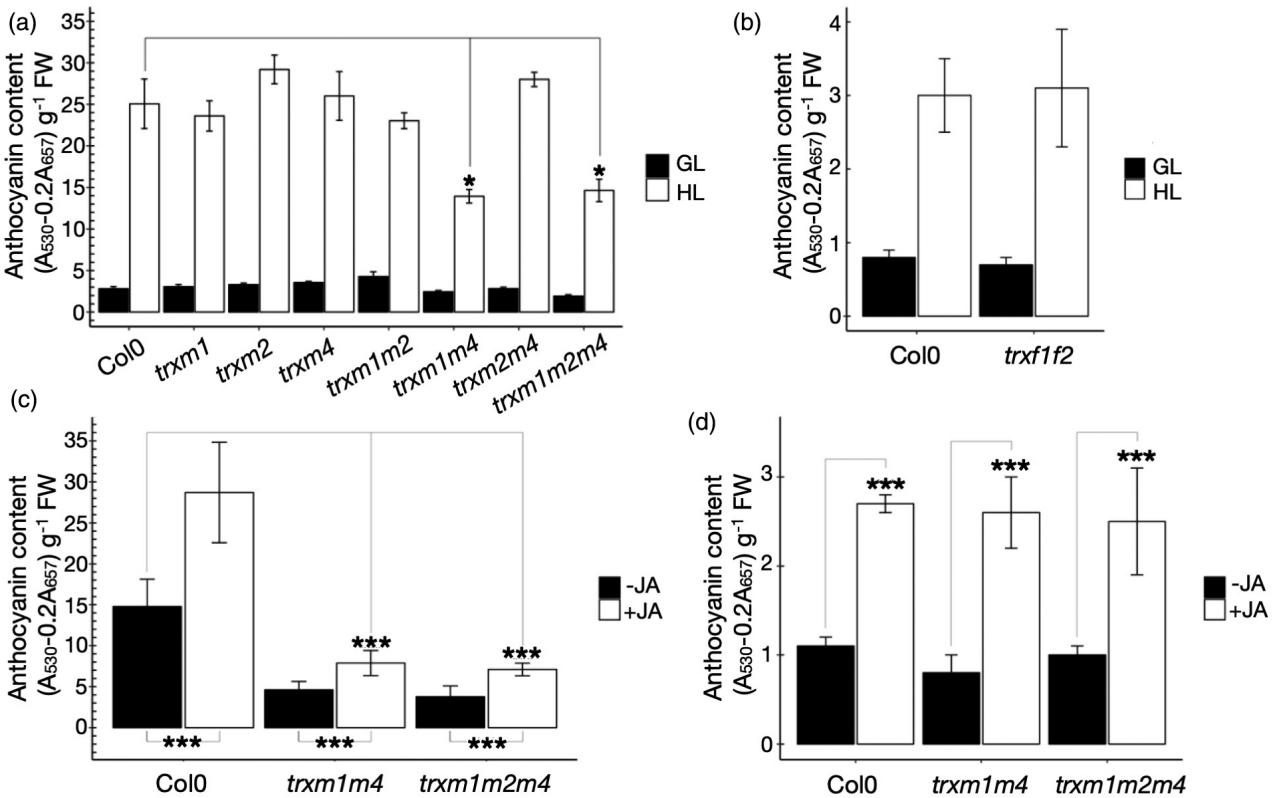

Figure 8. Anthocyanin accumulation in response to a high light (HL) treatment.
(a) Anthocyanin accumulation in 3-week-old wild-type (WT, Col0) and *trxm* plants after 4 days of an HL treatment.
(b) Anthocyanin accumulation in WT and *trxf1f2* mutant under the same experimental conditions as shown for (a).
(c) Anthocyanin accumulation in WT and *trxm1m4* and *trxm1m2m4* mutants after a 4-day HL treatment without (–JA) or with jasmonic acid (+JA).
(d) Anthocyanin accumulation in WT and *trxm1m4* and *trxm1m2m4* mutants cultivated under normal light conditions without (–JA) or with jasmonic acid (+JA). JA treatments consisted of spraying the leaves with a solution of 2 mM JA on the first and third days (twice a day) after initiating the HL incubation. Control plants (–JA) were treated with water. Data are presented as mean ± standard deviation. $*P < 0.05$, $***P < 0.01$ as analysed by one-way analysis of variance followed by a Tukey's *post hoc* test. $n = 5$ per genotype.

Peng et al., 2009; Yamori and Shikanai, 2016). Courteille et al. (2013) reported that TRX *m4* regulates both NDH- and PGR5-dependent CEF. However, the impairment suffered by PSII after an HL treatment seems to be independent from the regulation of CEF as all the TRX *m* isoforms were involved (though not equally), and not only TRX *m4*.

The pigment zeaxanthin is another key component of NPQ in plants. The lumen enzyme VDE catalyses the conversion of violaxanthin to zeaxanthin and its activity is inhibited when it is reduced (Hallin et al., 2015; Simionato et al., 2015). TRX *m* have been proposed to deliver electrons into the thylakoid lumen through CCDA and HCF164 (Motohashi and Hisabori, 2006, 2010) and, hence, indirectly may regulate enzymes such as VDE. Another TRX-regulated enzyme of the xanthophyll cycle is zeaxanthin epoxidase (ZE), which catalyses the conversion of zeaxanthin and antheraxanthin to regenerate violaxanthin. It has been reported that mutant plants lacking TRX *m* have higher levels of aggregated/inactivated ZE and accumulate high quantities of zeaxanthin (Da et al., 2018). The question that arises is whether the *trxm* lines display a high NPQ at medium light intensities (250 μmol photons m^{-2} sec^{-1}) instead of in HL (700 μmol photons m^{-2} sec^{-1}). One possibility is that, in HL, the low level of TRX *m* might be somewhat compensated after overcoming a reduction threshold or by the activation of unknown mechanisms restoring the energy assimilation balance at higher light intensities. Another possibility would consist of the existence of different energy dissipation mechanisms operating at different light intensities similarly to some transport proteins or enzyme isoforms that have different substrate affinities to cope with the fluctuating solute or substrate concentrations, which occur in the living systems.

Anthocyanin accumulation in response to HL depends on the TRX *m1* and *m4* redox regulation

Anthocyanins are protective pigments acting as a screening mechanism produced in response to a harmful

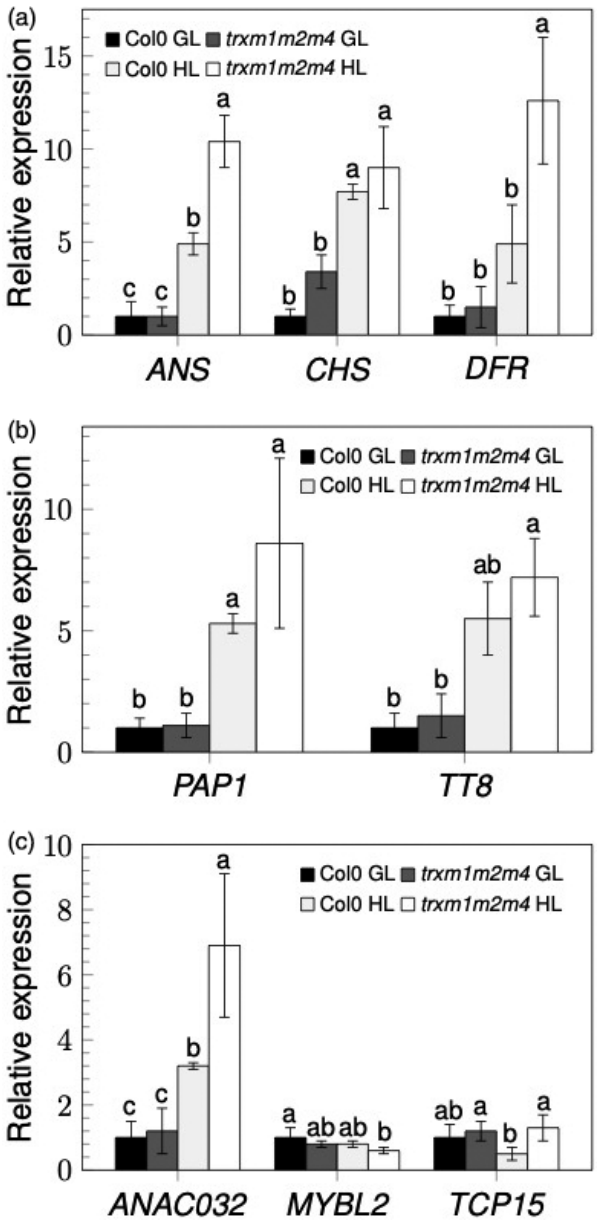

Figure 9. Transcript accumulation of anthocyanin biosynthesis and regulatory genes after a high light (HL) treatment.
(a) Quantitative polymerase chain reaction (qPCR) analysis of anthocyanin biosynthesis genes: anthocyanidin synthase (*ANS*), chalcone synthase (*CHS*), and dihydroflavonol-4-reductase (*DFR*).
(b) qPCR analysis of transcriptional activators of anthocyanin biosynthesis: Production of Anthocyanin Pigment 1 (*PAP1*) and Transparent Testa 8 (*TT8*).
(c) qPCR analysis of transcriptional repressors of anthocyanin biosynthesis: NAC transcription factor 32 (*ANAC032*), MYB-like 2 (*MYBL2*), and transcription factor TCP15 (*TCP15*). Three-week-old wild-type (Col0) and *trxm1m2m4* plants grown at growth light (GL) were exposed to a 4-day HL treatment. Data are presented as mean ± standard deviation. Different letters mean statistically significant difference according to a one-way analysis of variance followed by a Tukey's *post hoc* test. Three biological replicates were performed.

irradiation (Das et al., 2011). As far as we know, there are no previous reports about the influence of chloroplast TRXs in the regulation of the anthocyanin biosynthesis. According to the anthocyanin levels, it seems that either TRX *m1* or *m4* are necessary to trigger a full HL response, as we were unable to observe any difference between the single *trxm1* and *trxm4* mutants and the WT line. Moreover, both the double mutant *trxm1m4* as well as the triple mutant accumulated half the anthocyanin content of the WT line. Although we cannot rule out the possibility that the isoform TRX *m2* may also be contributing to this response, the fact is that the combination of the mutant allele *trxm2* with both other mutant alleles did affect other aspects of the plant physiology, casting doubts over the involvement of TRX *m2* in the anthocyanin response. Redox signalling originated from the chloroplast controls many aspects of plant cell biology. In this sense, the chloroplast TRXs, together with the proteins such as Executer 1 and 2, the thylakoid kinases STN7 and 8, and the plastoquinone pool, have been proposed as putative redox signalling players (Pfannschmidt et al., 2009).

We have proved that JA is not responsible for the impaired anthocyanin response in the *trxm1m4* mutants. Given that ZE, the first enzyme of the abscisic acid (ABA) biosynthesis pathway, largely tends to be inactivated in a *trxm* genetic background (Da et al., 2018), another likely possibility is that putative low levels of ABA may be impairing the anthocyanin response in the *trxm1m4* mutants (Li et al., 2019; Loreti et al., 2008). Nevertheless, we cannot rule out the possibility that TRX *m* may also have an ABA-independent signalling role in the response to HL, suggesting new research fields linking redox and hormonal regulation in plants.

Anthocyanin level was normal at GL in the triple *trxm* mutant (Figure 8a). We wondered whether anthocyanin-related genes did not respond properly to the light cue. To get more insight into this question we chose and analysed a group of HL-responding gene related to anthocyanin biosynthesis (Mahmood et al., 2016). Our results showed a misregulation of genes controlling anthocyanin biosynthesis (Figure 9b,c). Nevertheless, transcript levels of the biosynthesis genes were similar (*CHS*) or even more abundant (*ANS* and *DFR*) than in the WT line in response to HL (Figure 9a). We hypothesize that this over-response to HL would counterbalance a putative shortage of anthocyanin precursors. These results did not explain the observed phenotype and, despite our efforts, the question of how TRX *m* are regulating the anthocyanin accumulation in response to HL remains elusive.

Functional specialization of the TRX *m* isoforms Arabidopsis

During evolution, Arabidopsis multigenic families arose from gene-duplication events. In the case of the TRX-regulated proteins, the increasing target complexity led to a parallel diversification of the members of the TRX family. According to our results, the TRX *m1*, *m2*, and *m4* seem to

regulate a broad number of physiological processes, mainly integrating light and redox signalling. We have recently reported that many differentially expressed proteins in the *trxm* single mutants are related with photosynthetic proteins as well as with other extra-chloroplastic metabolic processes (Fernández-Trijueque et al., 2019).

We provide evidence about the significance of the redox signalling mediated by TRX *m* for the plant physiology; moreover, the diverse studies that we have carried out give solid clues about the ongoing specialization process inside this key subset of chloroplast TRXs. Despite having a plastid location, the broad range of affected processes suggests that these proteins are in the hub of the redox signalling controlling important plant traits, so far unreported, which are beyond the regulation of the chloroplast processes.

EXPERIMENTAL PROCEDURES

Plant material and growth conditions

Arabidopsis lines [Columbia (Col-0) genetic background] with T-DNA insertions in the TRX genes coding for the isoforms TRX *m1* (SALK_087118; Courteille et al., 2013; Wang et al., 2013), *m2* (SALK_130686; Fernández-Trijueque et al., 2019), *m4* (SALK_032538; Courteille et al., 2013; Wang et al., 2013), *f1* (SALK_128365; Okegawa and Motohashi, 2015; Fernández-Trijueque et al., 2019), and *f2* (GK_020E05; Fernández-Trijueque et al., 2019; Ojeda et al., 2017) were analysed.

Soil grown plants [peat soil/vermiculite (v/v) = 3:1], planted in standard plastic alveoli (180 ml capacity), were incubated in growth chambers under a long day photoperiod (16 h light–8 h dark) at 21°C/20°C (day/night) temperature and 60% relative humidity, and light intensities of 120 μmol photons m^{-2} sec^{-1} PAR for the optimal GL condition or 700 μmol photons m^{-2} sec^{-1} PAR for the HL condition, depending on the experimental conditions.

Plant genotyping

Single mutant lines (or a double and a single mutant line) were crossed, and homozygous double and triple lines were identified by polymerase chain reaction (PCR). Oligonucleotides are listed in Table S1.

Gas exchange measurements and PSII photochemical efficiency

The CO_2 assimilation rate was determined in the upper fully expanded leaf of the *A. thaliana* WT (Col-0) and simple, double, and triple *trxm* mutants by using a portable infrared gas analyser LI-6400 (LI-COR Biosciences, Inc., Lincoln, NE, USA), which allows the environmental conditions within the chamber (model 6400-02B LED Light Source) to be precisely controlled. The plantlets growth conditions were under HL and GL for 2 or 3 weeks and the *A* measurement was by changing light intensities (light curve), with a range of 0–2000 PAR (μmol photons m^{-2} sec^{-1}). The LI-6400 6.1 software was used to calculate the photosynthetic parameters.

The parameters of chlorophyll fluorescence emission (F_v/F_m) were determined by using a chlorophyll fluorometer PAM 2000 (Walz, Effeltrich, Germany). The maximum quantum yield of PSII (F_v/F_m) was calculated from the parameters using the following equation: $F_v/F_m = (F_m - F_0)/F_m$, where F_0 is the initial minimal fluorescence emitted from leaves dark-adapted for 15 min and F_m the maximal fluorescence elicited by saturating actinic light.

In plants subjected to a 2-day HL treatment, chlorophyll *a* fluorescence was monitored using the Walz maxi-imaging-PAM. Saturation pulses (2700 μmol photons m^{-2} sec^{-1} for 0.8 sec) were applied to determine F_m and F'_m. Y(II) was calculated as $F'_m - F'/F'_m$, q_L as $(F'_m - F)/(F'_m - F'_0) \times F'_0/F$, and NPQ was calculated as $(F_m - F'_m)/F'_m$ where the value of F_m was determined after relaxation of NPQ for 15 min in the dark, as described in Li et al. (2002).

Light and scanning electron microscopy

Semi-thin sections of 1 mm of Col-0 and *trxm* mutants of Arabidopsis leaves grown under GL or HL were processed as described in Barajas-López et al. (2007). After staining with toluidine blue the tissue structure was visualized in an OLYMPUS BX51 light microscope.

The number, shape, and opening of the stomata were observed and measured in the leaf adaxial and abaxial epidermis of at least three plants per line by using High Resolution Scanning Electron Microscopy AURIGA (Carl Zeiss SMT, Jena, Germany). High resolution and low voltages images of secondary electron taken by a secondary electron in-lens detector of 500-fold magnification were analysed for stomata quantification and size measuring with ImageJ software.

Anthocyanin extraction and quantification

Leaf samples were incubated overnight at 4°C in the dark with acidic methanol (1% HCl v/v). The samples were centrifuged, and the absorbance of the supernatants was measured at 530 and 657 nm. According to Rabino and Mancinelli (1986), anthocyanin content was calculated as $(A_{530} - 0.2A_{657})$ g^{-1}fresh weight.

Total RNA extraction, cDNA synthesis, and quantitative reverse transcriptase-polymerase chain reaction (RT-PCR) analysis

Total RNA was isolated using the TRIzol™ Reagent (Thermo Fisher Scientific, Waltham, MA, USA) and cDNA synthesis was carried out with the PrimeScript™ RT Master Mix (Takara Bio, Shiga, Japan) according to the manufacturers' instructions. Real-time RT-PCR was performed using the TB Green Premix Ex Taq (Takara Bio) following the manufacturer's protocol. Expression values from two technical and three biological replicates were analysed using the $2^{-\Delta\Delta CT}$ method (Livak and Schmittgen, 2001). *UBI10* was used as an internal reference gene for normalization. Oligonucleotides used are listed in Table S1.

Statistical analysis

Statistical analyses of data were performed using R software (https://rstudio.com). Significant differences between groups were tested using the analysis of variance test and the pairwise comparison Tukey HSD test with the "Agricolae package" (available online at: https://CRAN.R-project.org/package=agricola). Manhattan distance (rectilinear distance, abbreviated as "dm") were calculated as $d_{man}(p, q) = \sum_{i=1}^{n} |(p_i - q_i)|$, the sum of the absolute differences between points (p_i and q_i) of different curves.

Accession numbers

AT1G03680, *TRXm1*; AT2G15570, *TRXm2;* AT1G50320, *TRXm4*; AT3G02730, *TRXf1*; AT5G16400, *TRXf2*; *PAP1*, AT1G56650; *TT8*, AT4G09820; *TCP15*, AT1G69690; *ANAC032*, AT1G77450; *MYBL2*, AT1G71030; *CHS*, AT5G13930; *DFR*, AT5G42800; and *ANS*, AT2G38240.

ACKNOWLEDGEMENTS

The authors thank Tamara Molina for her technical support, and Angela Tate for helpful editorial feedback on the manuscript. The microscopy assays and observations were carried out at the Scientific Instrumentation Centre of the University of Granada (Spain). This research was funded by research projects BIO2015-65272-C2-1-P, from the Spanish Ministry of Economy and Competitiveness (MINECO) and the European Fund for Regional Development and PGC2018-096851-B-C21, from the Spanish Ministry of Science, Innovation and Universities (MICINN) and the European Fund for Regional Development.

AUTHOR CONTRIBUTIONS

AJS, AM, and MS designed the research; AJS obtained the double and triple mutant lines and specific antibodies; JAR-G and AJS carried out the photosynthesis measurements and data analyses, MS and AJS the microscopy analyses, DT-R and AM the chlorophyll fluorescence analyses, AJS and PV the anthocyanin and qPCR analyses, AJS, AM, and MS analysed the data, AJS wrote the article and MS and AM revised the article; all the authors have read and approved the final article.

CONFLICT OF INTERESTS

The authors declare that they have no competing interests.

DATA AVAILABILITY STATEMENT

Data from this study can be provided by the corresponding author upon request.

SUPPORTING INFORMATION

Additional Supporting Information may be found in the online version of this article.

Figure S1. T-DNA insertions and immunodetection of TRX *m* by using specific antibodies in the *trxm* genetic backgrounds.

Figure S2. Relative TRX *m* content in WT plants grown in GL and in HL. Three biological replicates were performed for the quantification.

Figure S3. Light-response curves of PSII quantum yield (Y(II)), non-photochemical quenching (NPQ), and open reaction centres in PSII (1-q_L) in wild-type (Col-0) and single *trxm* mutants. The plants were grown at optimal growth light (GL) and then subjected to a 2-day high light (2-day HL) treatment. Next, the plants were taken back to GL conditions to allow stress recovery, measuring chlorophyll fluorescence 1 day (1-day RV) and 1 week after (7-day RV). Data are presented as mean ± SE. Four biological replicates were performed.

Table S1. Oligonucleotides used for determination of Arabidopsis mutant genotypes and qPCR analyses.

Table S2. Photosynthetic parameters of the WT and *trxm* mutant lines.

Data S1. Supporting Experimental Procedures

REFERENCES

Balfagón, D., Sengupta, S., Gómez-Cadenas, A., Fritschi, F.B., Azad, R.K., Mittler, R. *et al.* (2019) Jasmonic acid is required for plant acclimation to a combination of high light and heat stress. *Plant Physiology*, **181**, 1668–1682.

Barajas-López, J.D., Serrato, A.J., Olmedilla, A., Chueca, A. & Sahrawy, M. (2007) Localization in roots and flowers of pea chloroplastic thioredoxin *f* and thioredoxin *m* proteins reveals new roles in non photosynthetic organs. *Plant Physiology*, **145**, 946–960.

Benitez-Alfonso, Y., Cilia, M., San Roman, A., Thomas, C., Maule, A., Hearn, S. *et al.* (2009) Control of Arabidopsis meristem development by thioredoxin-dependent regulation of intercellular transport. *Proceedings of the National Academy of Sciences of the United States of America*, **106**, 3615–3620.

Brooks, M.D., Sylak-Glassman, E.J., Fleming, G.R. & Niyogi, K.K. (2013) A thioredoxin-like/β-propeller protein maintains the efficiency of light harvesting in Arabidopsis. *Proceedings of the National Academy of Sciences of the United States of America*, **110**, 2733–2740.

Chi, Y.H., Moon, J.C., Park, J.H., Kim, H.-S., Zulfugarov, I.S., Fanata, W.I. *et al.* (2008) Abnormal chloroplast development and growth inhibition in rice thioredoxin *m* knock-down plants. *Plant Physiology*, **148**, 808–817.

Collin, V., Issakidis-Bourguet, E., Marchand, C., Hirasawa, M., Lancelin, J.-M., Knaff, D.B. *et al.* (2003) The Arabidopsis plastidial thioredoxins: new functions and new insights into specificity. *Journal of Biological Chemistry*, **278**, 23747–23752.

Courteille, A., Vesa, S., Sanz-Barrio, R., Cazalé, A.-C., Becuwe-Linka, N., Farran, I. *et al.* (2013) Thioredoxin *m4* controls photosynthetic alternative electron pathways in Arabidopsis. *Plant Physiology*, **161**, 508–520.

Da, Q., Sun, T., Wang, M., Jin, H., Li, M., Feng, D. *et al.* (2018) M-type thioredoxins are involved in the xanthophyll cycle and proton motive force to alter NPQ under low-light conditions in Arabidopsis. *Plant Cell Reports*, **37**, 279–291.

Das, P.K., Geul, B., Choi, S.-B., Yoo, S.-D. & Park, Y.-I. (2011) Photosynthesis-dependent anthocyanin pigmentation in Arabidopsis. *Plant Signaling & Behavior*, **6**, 23–25.

Fernández-Trijueque, J., Serrato, A.J. & Sahrawy, M. (2019) Proteomic analyses of thioredoxins *f* and *m* *Arabidopsis thaliana* mutants indicate specific functions for these proteins in plants. *Antioxidants*, **8**, 54.

Gollan, P.J., Tikkanen, M. & Aro, E.M. (2015) Photosynthetic light reactions: integral to chloroplast retrograde signalling. *Current Opinion in Plant Biology*, **27**, 180–191.

Gütle, D.D., Roret, T., Hecker, A., Reski, R. & Jacquot, J.P. (2017) Dithiol disulphide exchange in redox regulation of chloroplast enzymes in response to evolutionary and structural constraints. *Plant Science*, **255**, 1–11.

Hallin, E.I., Guo, K. & Åkerlund, H.E. (2015) Violaxanthin de-epoxidase disulphides and their role in activity and thermal stability. *Photosynthesis Research*, **124**, 191–198.

Hoshino, R., Yoshida, Y. & Tsukaya, H. (2019) Multiple steps of leaf thickening during sun-leaf formation in Arabidopsis. *The Plant Journal*, **100**, 738–753.

Kang, Z., Qin, T. & Zhao, Z. (2019) Thioredoxins and thioredoxin reductase in chloroplasts: a review. *Gene*, **706**, 32–42.

Kang, Z.H. & Wang, G.X. (2016) Redox regulation in the thylakoid lumen. *Journal of Plant Physiology*, **192**, 28–37.

Karamoko, M., Cline, S., Redding, K., Ruiz, N. & Hamel, P.P. (2011) Lumen thiol oxidoreductase1, a disulfide bond-forming catalyst, is required for the assembly of photosystem II in Arabidopsis. *The Plant Cell*, **23**, 4462–4475.

Laughlin, T.G., Bayne, A.N., Trempe, J.F., Savage, D.F. & Davies, K.M. (2019) Structure of the complex I-like molecule NDH of oxygenic photosynthesis. *Nature*, **566**, 411–414.

Lemaire, S.D., Michelet, L., Zaffagnini, M., Massot, V. & Issakidis-Bourguet, E. (2007) Thioredoxins in chloroplasts. *Current Genetics*, **51**, 343–365.

Li, G., Zhao, J., Qin, B., Yin, Y., An, W., Mu, Z. *et al.* (2019) ABA mediates development-dependent anthocyanin biosynthesis and fruit coloration in *Lycium* plants. *BMC Plant Biology*, **19**, 317.

Li, X.P., Muller-Moule, P., Gilmore, A.M. & Niyogi, K.K. (2002) PsbS-dependent enhancement of feedback de-excitation protects photosystem II from photoinhibition. *Proceedings of the National Academy of Sciences of the United States of America*, **99**, 15222–15227.

Livak, K.J. & Schmittgen, T.D. (2001) Analysis of relative gene expression data using real-time quantitative PCR and the 2(-Delta Delta C(T)) method. *Methods*, **25**, 402–408.

Loreti, E., Povero, G., Novi, G., Solfanelli, C., Alpi, A. & Perata, P. (2008) Gibberellins, jasmonate and abscisic acid modulate the sucrose-induced

expression of anthocyanin biosynthetic genes in *Arabidopsis*. *New Phytologist*, **179**, 1004–1016.

Mahmood, K., Xu, Z., El-Kereamy, A., Casaretto, J.A. & Rothstein, S.J. (2016) The Arabidopsis transcription factor ANAC032 represses anthocyanin biosynthesis in response to high sucrose and oxidative and abiotic stresses. *Frontiers in Plant Science*, **7**, 1548.

Massonnet, C., Vile, D., Fabre, J., Hannah, M.A., Caldana, C., Lisec, J. *et al.* (2010) Probing the reproducibility of leaf growth and molecular phenotypes: a comparison of three Arabidopsis accessions cultivated in ten laboratories. *Plant Physiology*, **152**, 2142–2157.

Meyer, Y., Buchanan, B.B., Vignols, F. & Reichheld, J.P. (2009) Thioredoxins and glutaredoxins: unifying elements in redox biology. *Annual Review of Genetics*, **43**, 335–367.

Motohashi, K. & Hisabori, T. (2006) HCF164 receives reducing equivalents from stromal thioredoxin across the thylakoid membrane and mediates reduction of target proteins in the thylakoid lumen. *Journal of Biological Chemistry*, **281**, 35039–35047.

Motohashi, K. & Hisabori, T. (2010) CcdA is a thylakoid membrane protein required for the transfer of reducing equivalents from stroma to thylakoid lumen in the higher plant chloroplast. *Antioxidants & Redox Signaling*, **13**, 1169–1176.

Müller, P., Li, X.P. & Niyogi, K.K. (2001) Non-photochemical quenching. A response to excess light energy. *Plant Physiology*, **125**, 1558–1566.

Munekage, Y., Hashimoto, M., Miyake, C., Tomizawa, K.I., Endo, T., Tasaka, M. *et al.* (2004) Cyclic electron flow around photosystem I is essential for photosynthesis. *Nature*, **429**, 579–582.

Munekage, Y., Hojo, M., Meurer, J., Endo, T., Tasaka, M. & Shikanai, T. (2002) PGR5 is involved in cyclic electron flow around photosystem I and is essential for photoprotection in Arabidopsis. *Cell*, **110**, 361–371.

Naranjo, B., Mignée, C., Krieger-Liszkay, A., Hornero-Méndez, D., Gallardo-Guerrero, L., Cejudo, F.J. *et al.* (2016) The chloroplast NADPH thioredoxin reductase C, NTRC, controls non-photochemical quenching of light energy and photosynthetic electron transport in Arabidopsis. *Plant, Cell and Environment*, **39**, 804–822.

Nikkanen, L. & Rintamäki, E. (2019) Chloroplast thioredoxin systems dynamically regulate photosynthesis in plants. *The Biochemical Journal*, **476**, 1159–1172.

Nikkanen, L., Toivola, J. & Rintamäki, E. (2016) Crosstalk between chloroplast thioredoxin systems in regulation of photosynthesis. *Plant, Cell and Environment*, **39**, 1691–1705.

Ojeda, V., Pérez-Ruiz, J.M., González, M., Nájera, V.A., Sahrawy, M., Serrato, A.J. *et al.* (2017) NADPH thioredoxin reductase C and thioredoxins act concertedly in seedling development. *Plant Physiology*, **174**, 1436–1448.

Okegawa, Y. & Motohashi, K. (2015) Chloroplastic thioredoxin *m* functions as a major regulator of Calvin cycle enzymes during photosynthesis *in vivo*. *The Plant Journal*, **84**, 900–913.

Peng, L., Fukao, Y., Fujiwara, M., Takami, T. & Shikanai, T. (2009) Efficient operation of NAD(P)H dehydrogenase requires supercomplex formation with photosystem I via minor LHCI in Arabidopsis. *The Plant Cell*, **21**, 3623–3640.

Pfannschmidt, T., Bräutigam, K., Wagner, R., Dietzel, L., Schröter, Y., Steiner, S. *et al.* (2009) Potential regulation of gene expression in photosynthetic cells by redox and energy state: approaches towards better understanding. *Annals of Botany*, **103**, 599–607.

Rabino, I. & Mancinelli, A.L. (1986) Light, temperature, and anthocyanin production. *Plant Physiology*, **81**, 922–924.

Ren, T., Weraduwage, S.M. & Sharkey, T.D. (2019) Prospects for enhancing leaf photosynthetic capacity by manipulating mesophyll cell morphology. *Journal of Experimental Botany*, **70**, 1153–1165.

Schürmann, P. & Buchanan, B.B. (2008) The ferredoxin/thioredoxin system of oxygenic photosynthesis. *Antioxidants & Redox Signaling*, **10**, 1235–1274.

Serrato, A.J., Fernández-Trijueque, J., Barajas-López, J.D., Chueca, A., Sahrawy, M. & Reichheld, J.P. (2013) Plastid thioredoxins: a "one-for-all" redox-signaling system in plants. *Frontiers in Plant Science*, **4**, 463.

Shan, X., Zhang, Y., Peng, W., Wang, Z. & Xie, D. (2009) Molecular mechanism for jasmonate-induction of anthocyanin accumulation in Arabidopsis. *Journal of Experimental Botany*, **60**, 3849–3860.

Simionato, D., Basso, S., Zaffagnini, M., Lana, T., Marzotto, F., Trost, P. *et al.* (2015) Protein redox regulation in the thylakoid lumen: the importance of disulfide bonds for violaxanthin de-epoxidase. *FEBS Letters*, **589**, 919–923.

Thormählen, I., Zupok, A., Rescher, J., Leger, J., Weissenberger, S., Groysman, J. *et al.* (2017) Thioredoxins play a crucial role in dynamic acclimation of photosynthesis in fluctuating light. *Molecular Plant*, **10**, 168–182.

Wang, P., Liu, J., Liu, B., Feng, D., Da, Q., Shu, S. *et al.* (2013) Evidence for a role of chloroplastic *m*-type thioredoxins in the biogenesis of photosystem II in Arabidopsis. *Plant Physiology*, **163**, 1710–1728.

Yamori, W. & Shikanai, T. (2016) Physiological functions of cyclic electron transport around photosystem I in sustaining photosynthesis and plant growth. *Annual Review of Plant Biology*, **67**, 81–106.

Zhang, M., Takano, T., Liu, S. & Zhang, X. (2015) Arabidopsis mitochondrial voltage-dependent anion channel 3 (AtVDAC3) protein interacts with thioredoxin *m2*. *FEBS Letters*, **589**, 1207–1213.